American Mineralogist, Volume 76, pages 49–59, 1991

The hydroxide component in synthetic pyrope

Charles A. Geiger,* Klaus Langer
Institut für Mineralogie und Kristallographie, Technische Universität Berlin, Ernst-Reuter-Platz 1, D-1000 Berlin 12, Germany
David R. Bell, George R. Rossman
Division of Geological and Planetary Sciences, California Institute of Technology, Pasadena, California 91125, U.S.A.
Björn Winkler**
Technische Universität Berlin, Ernst-Reuter-Platz 1, D-1000 Berlin 12, Germany

Abstract

A series of pyrope single crystals up to 2 mm in size was synthesized over a range of hydrothermal pressures of 20.0 to 50.0 kbar and temperatures of 800 to 1200 °C using different starting materials (oxides, glass, gel) and fluid fluxes (H_2O, NaOH, HCl). The crystals were characterized by optical, SEM, microprobe, and X-ray techniques. Single crystal Fourier-transform infrared (FTIR) spectroscopy was used to measure the incorporated structural OH^-. Spectra measured in the region of 4000–3000 cm^{-1} wavenumbers were different for all samples grown from oxides or glass vs. those grown from the gel at temperatures less than 1000 °C. In spectra obtained at room temperature the former are characterized by a single OH^- stretching vibration at 3629 cm^{-1}, full widths at half-height (FWHH) = 60 cm^{-1}, which is present regardless of the synthesis conditions (P,T or fluid flux). At 78 K, the single band splits into two narrow bands of FWHH of 11 cm^{-1} each. The unit-cell dimension of pyrope increases up to 0.004 Å with the incorporation of OH^-. The best interpretation of these data is that OH^- defects are introduced into the pyrope structure as a hydrogarnet component where $(O_4H_4)^{4-} = SiO_4^{4-}$, i.e., by the substitution $Si^{4+} + 4O^{2-} = {}^{[4]}\square + 4OH^-$. The amount of OH^- substitution into pyrope ranges from 0.02 to 0.07 wt% expressed as H_2O. The infrared (IR) spectra of pyropes grown from a gel starting material, at temperatures less than 1000 °C, display four band spectra, which indicate that OH^- substitution is not governed solely by the hydrogarnet substitution. Natural pyrope-rich garnets generally have lower OH^- concentrations and more complicated IR spectra than the synthetic pyrope crystals grown from oxides. This is assumed to be caused by crystal chemistry differences and probably different mechanisms of OH^- incorporation.

Introduction

Pyrope garnet, $Mg_3Al_2Si_3O_{12}$, is only stable at elevated pressures and is nominally an anhydrous phase of cubic structure, with space group $Ia3d$. Rigorous understanding of the crystallochemical properties of pyrope is not only of mineralogical interest, but also has an important bearing on petrological and geophysical processes. It has been shown that both synthetic end-member pyropes (Ackermann et al., 1983; Begley and Sclar, 1984; Geiger et al., 1989b) and natural pyrope-rich garnets (Aines and Rossman, 1984a, 1984b) contain small amounts of structural OH^- often loosely referred to as water. Pyrope-rich garnets constitute a portion of the earth's mantle and therefore, the bulk H_2O content in the earth's interior is partly a function of H_2O held in garnet. Petrologic processes involving, for example, metasomatism and melting could be influenced by garnet containing OH^-. The presence of OH^- could also affect the physical properties of garnet and, hence, the rheological properties of the mantle.

There are several outstanding questions regarding the presence of OH^- in synthetic pyrope and natural pyrope-rich garnets.

1. Where are the OH^- groups bound in the pyrope structure? It is frequently assumed that the OH^- is substituted as the classic hydrogarnet substitution, where $(H_4O_4)^{4-} = SiO_4^{4-}$, but this has not yet been demonstrated. Substitutional mechanisms other than the hydrogarnet substitution are possible and have been proposed in the case of hydrogrossular garnet (Basso et al., 1984), but have yet to be proven for pyrope.

2. What are the limits of OH^- substitution in synthetic pyrope and how is the concentration influenced by growth conditions and external variables, i.e., P, T, f_{H_2O}?

3. How do the OH^- contents and substitutional mech-

* Present address: Bayerisches Forschungsinstitut für Experimentelle Geochemie und Geophysik, Universität Bayreuth, Postfach 10 12 51, 8580 Bayreuth, Germany.
** Present address: Department of Earth Sciences, University of Cambridge, Cambridge, CB2 3EQ, U.K.

0003–004X/91/0102–0049$02.00

anisms of synthetic pyrope compare to those of natural pyrope and to those of other synthetic garnets (i.e., grossular and almandine)?

The principal analytical technique used to detect and measure the OH^- contents in nominally anhydrous silicates is infrared (IR) spectroscopy, as recently reviewed by Rossman (1988). Unfortunately, this method does not give direct and exact structural information on the location of the protons. The OH^- contents in natural or synthetic pyrope are too low (Ackermann et al., 1983; Aines and Rossman, 1984b) to be detected by present X-ray, neutron diffraction, or H^+-NMR techniques, and therefore direct structural information on the positions of the H^+ is lacking. However, recent developments in Fourier-transform IR (FTIR) spectroscopy permit more accurate and higher resolution measurements to be made on small single crystals. This allows previous uncertainties and discrepancies in the literature to be resolved and new structural inferences regarding the location of the OH^- groups and their concentrations to be made.

Previous work

Ackermann et al. (1983) were the first to show that small amounts of OH^- could be found in hydrothermally prepared synthetic pyrope single crystals. They presented IR spectra obtained on a microscope IR device using an interference filter monochromator, where the accuracy and resolution are not as good as is presently possible with the new FTIR spectrometers. In addition, most of their spectra were dominated by a broad band resulting from molecular H_2O held in tiny fluid inclusions, which masked the weaker OH^- band. They detected a single OH^- stretching vibration located at 3600 cm^{-1}. They estimated that the absolute OH^- in their pyrope samples was in the range of 0.05 wt% expressed as H_2O.

Aines and Rossman (1984a, 1984b) made a systematic study of OH^- in natural pyralspite garnets from a variety of geologic environments. They measured the IR spectra using a conventional grating spectrometer on optically clear crystals using small apertures on 1 mm or thicker platelets at both room and liquid N_2 temperatures. They detected OH^- in nearly all of the pyropic garnets studied, including those of mantle origin. In contrast to the work of Ackermann et al. (1983), they proposed that two OH^- stretching bands located at approximately 3660 and 3560 cm^{-1} were characteristic of pyrope-rich garnets. They estimated that the H_2O content of their pyrope samples ranged from 0.0 up to 0.26 wt% H_2O, and they suggested that this range was a result of different intrinsic H_2O fugacities in the mantle source region where the garnets grew or equilibrated.

On the basis of these two studies, there are differences between natural and synthetic pyrope garnets as to both the number and positions of the OH^- stretching bands. It was argued that the OH^- bands observed in the synthetic pyrope garnets may be a result of included solid phases (Aines and Rossman, 1984b). A primary aim of this study is to make further measurements, using micro-FTIR techniques, of synthetic pyrope so that differences between natural and synthetic pyropes can be understood. In particular, we hope to address the general questions listed above and the following specific questions. (1) How many IR active OH^- stretching bands are present in the spectra of synthetic pyrope containing small amounts of OH^-, and are the experimental spectroscopic observations in agreement with the theoretical predictions based on site group calculations? (2) What are the positions of these bands and do they change as a function of composition or P and T of synthesis? (3) Do the OH^- contents of synthetic pyropes represent equilibrium values incorporated at P, T and f_{H_2O} during growth? (4) Are the OH^- contents a function of the P and T of synthesis?

Experimental methods

Synthesis

Synthetic pyrope single crystals were grown using three different starting materials: an oxide mixture, a glass, and gels. The oxide mixture was prepared by grinding an intimate mixture of MgO (99.999%, Ventron, Alfa Product), SiO_2 (99.99%, Koch-Light Laboratories) and Al_2O_3 (99.9999%, Koch-Light Laboratories) powders of stoichiometric pyrope composition under H_2O in an agate mortar for about 2 h. The oxides were fired at 1000 °C for several hours and then stored in a desiccator prior to weighing. The glass of pyrope composition was prepared by melting a similarly prepared oxide mixture at 1620 °C in platinum crucibles and quenching it in H_2O (Geiger et al., 1987). The pyrope gel used in Berlin was the same as that used in the study of Ackermann et al. (1983). Syntheses at Pasadena were conducted solely with the gel technique. The gel was provided by P. J. Wyllie (Sekine et al., 1981).

Pyrope single crystals were grown hydrothermally in a piston-cylinder device in Au or Pt capsules with outer dimensions of 3.5 mm diameter and 5 mm long or 5.5 mm diameter and 10 mm long, and placed in a 26-mm-diameter salt-based high pressure assembly described in Cemič et al. (1990). Experiments above 25 and below 31 kbar were made in an 18 mm assembly consisting of an outer salt sleeve with inner parts fabricated from salt or boron nitride. Syntheses at Cal Tech were conducted using Au capsules and a half-inch NaCl-based furnace assembly. For syntheses above 30 kbar a 0.5 in. assembly, similar to the type I cell of Massonne and Schreyer (1986), was used at Bochum University, except that the capsule was situated vertically below the thermocouple. We estimate that the temperatures are accurate to ±10 °C and the nominal pressures differ by no more than 1 kbar from the true pressures. Several experiments were also made using 1N NaOH and dilute HCl as the fluid flux together with the oxide mix. The ratio of solids to fluid varied slightly, but was normally between 4 and 6 to 1, by weight. A couple of syntheses were also made using an oxide mixture containing 10 wt% excess SiO_2.

The experimental conditions varied from 800 to 1200

TABLE 1. Synthesis conditions of the pyropes used in this study

Sample	Pressure (kbar)	Temperature (°C)	Duration (h)	Starting material	Fluid	Fluid/solid ratio (g)
P-5	23.9	1000	24	oxides	H_2O	0.008/0.031
P-7	23.9	1000	48	glass	H_2O	0.008/0.037
P-8	23.9	1000	24	gel	H_2O	0.007/0.037
P-13	22.9	1100	20	oxides	H_2O	0.009/0.034
P-18	25.8	1000	16	oxides	H_2O	—
P-27	20.0	900	20	gel	H_2O	0.0004/0.030
P-29	24.0	950	36	oxides	H_2O	0.026/0.162
P-44	22.0	1025	18	oxides	HCl	0.008/0.0399
P-51	24.0	1000	19	oxides + silica	H_2O	0.025/0.150
P-54	40.0	1000	18	oxides	H_2O	0.022/0.150
P-57	45.0	1000	3	oxides	H_2O	0.008/0.043
P-69	50.0	800	24	gel	H_2O	0.007/0.025
P-77	35.0	1000	2.5	oxides + silica	H_2O	0.008/0.033
P-90	30.0	900	48	oxides	H_2O	0.007/0.036
P-94	30.0	1000	50	oxides	NaOH	0.006/0.041
DB-31	20.0	1000	100	gel	H_2O	—
DB-30	25.0	1000	100	gel	H_2O	—

Note: The samples from the P series were made in Berlin and those from DB in Pasadena.

°C and from 20 to 50 kbar. The durations of the experiments were from several hours up to 4 d. Upon opening, the capsules were always examined for a liquid to ensure that a fluid phase was present during crystal growth. Capsules that had leaked or did not show the presence of a fluid were discarded. Table 1 lists the synthesis conditions of the crystals used in this study.

Characterization and FTIR spectroscopy

The experimental products were examined by optical microscope, X-ray powder diffraction, electron microprobe, and SEM techniques. Routine X-ray measurements using smear mounts on glass slides were undertaken to detect additional phases coexisting with the pyrope crystals in most of the syntheses. Powder refinements were also made on several crushed and ground pyrope single crystals. Data were collected from 10° to 100° 2θ using Cu$K\alpha_1$ radiation on a Stoe diffractometer. Powdered Si from the U.S. National Bureau of Standards was used as an internal standard. The spectra were fit assuming lorenzian squared line shapes and refined using a least-squares program.

Analyses (WDS) using a Cameca microprobe were made on representative crystals, mostly the same ones used in the FTIR measurements. Synthetic oxides (MgO and Al_2O_3) and natural wollastonite for Si were used as standards. Several line scans across the crystals were made to check for chemical zonation, otherwise random spot analyses were made. The beam size was 2–10 μm in diameter with an accelerating voltage of 15 kV and a beam current of 20 nA measured with a Faraday cup. The data correction program employed was supplied by Cameca and entitled PAP (Pouchoux and Pichoire).

For the IR measurements, pyrope crystals were selected from a given synthesis that were generally the largest and most euhedral and contained the least amount of solid inclusions. The single crystals were embedded in epoxy and ground and polished on both sides to obtain crystal platelets with thicknesses ranging from approximately 50 up to 700 μm, with most between 100 and 250 μm (Fig. 1). These single crystal mounts were used for microscopic examination and also for the microscopic FTIR measurements. This method of preparation allowed us to examine the crystals optically for both solid and liquid inclusions and to make IR measurements across crystals of known and constant thickness without spectral interference from epoxy or glass.

The IR measurements were made on two different spectrometers. The device used at Caltech was a Nicolet 60SX FTIR spectrometer, and the measurements were made at a resolution of 2 to 4 cm^{-1} using an InSb detector. The experimental arrangement consists of attaching circular apertures of various sizes (approximately 50–150 μm in diameter) directly onto the ground and polished crystals held in the epoxy mounts and, after careful alignment in the IR beam, measuring generally between 1000 and 2000 spectra. Measurements made at 78 K were made on this spectrometer using a home-made liquid N_2 cell. The second spectrometer employed was a Bruker FTIR 66 model equipped with a microscope. A variety of measuring sizes were used ranging from 50 × 50 to 10 × 10 μm at a resolution of 2 to 4 cm^{-1} using a HgCdTe detector. 15 × or 36 × objectives were used. The background measurement in the latter was made in air and in the former within the spectrometer using air that had been dried and purged of CO_2.

RESULTS

Product materials

A variety of synthetic pyrope single crystals was grown. Crystal sizes ranged from 0.05 to 2 mm. The crystals were typically subhedral to euhedral with forms {110} or {110} and {211} present. The largest single crystals were grown at pressures in excess of 20 kbar (Table 1) from the oxide mixture. They frequently nucleated along the walls of the

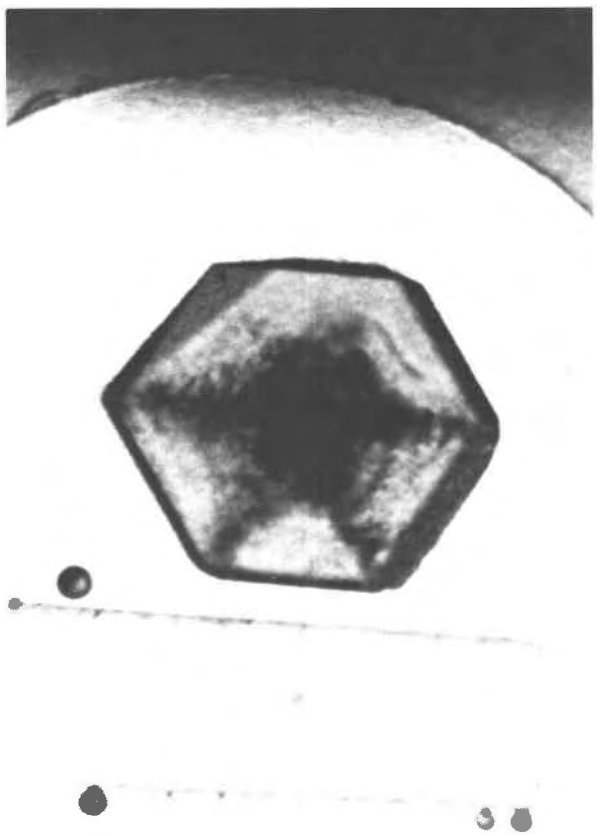

Fig. 1. Plane light photograph showing a typical mount used for optical microscopic examination and the FTIR measurements. The top crystal is pyrope and the bottom a quartz platelet oriented parallel to the *c*-axis. Note the inclusion pattern in the pyrope crystal. The crystal is approximately 1.3 mm across from corner to corner.

capsule. In many syntheses using oxides the capsule contained large pyrope crystals, surrounded by a finer-grained matrix consisting of a complex variety of other phases (i.e., enstatite, forsterite, chlorite, etc.) within the system MgO-Al_2O_3-SiO_2-H_2O. These additional phases were highly variable in abundance and modal proportions, and their occurrence depended upon the pressure and temperature conditions and duration of the syntheses. They were more prevalent at the lower temperatures. Pyrope crystals could not be grown from the oxide mixture at temperatures less than 900 °C. For syntheses at lower temperature the gel and glass were employed. Pyrope crystals grown from the glass and gel were typically smaller in size than those grown from oxide mix, but these starting materials resulted in more complete yields of pyrope. The largest euhedral single crystals produced were grown around 1000 ± 50 °C at 25 ± 5 kbar. SEM photographs of pyrope single crystals grown from the three different starting materials are shown in Figure 2.

Table 2. Unit-cell dimensions of synthetic pyrope

a_o (Å)	Pressure (kbar)	Temperature (°C)	Synthesis conditions
11.4540 (5)-*R*	30	1350–1400	dry from glass[1]
11.454 (1)	30	1400	dry from glass[2]
11.457 (1)-*R*	37	1000	hydrothermal[3]
11.456 (1)	36	1300	hydrothermal[4]
11.4568 (3)	25	1000	hydrothermal[5]
11.464 (1)-*R*	25	1000	hydrothermal[6]
11.457 (1)-*R*	40	1300	dry from glass[7]
11.459 (1)	30	1370	dry from glass[8]
11.459 (1)	unspecified		oxides[9]
11.456 (2)	30	1300	hydrothermal[10]
11.4579 (3)	25	1000	hydrothermal[11]
11.457 (1)-*R*	25	1000	hydrothermal[12]
11.458 (1)-*R*	45.0	1000	hydrothermal (P-57)[13]
11.458 (1)-*R*	50.0	800	hydrothermal (P-69)[13]
11.457 (1)-*R*	23.9	1000	hydrothermal (P-8)[13]
11.457 (1)-*R*	40.0	1000	hydrothermal (P-54)[13]

[1] Haselton and Westrum (1980).
[2] Geiger et al. (1987).
[3] Akaogi and Akimoto (1977).
[4] Hazen and Finger (1978).
[5] Ackermann et al. (1983).
[6] Schreyer and Seifert (1969).
[7] Newton et al. (1977).
[8] Wood (1988).
[9] Skinner (1956).
[10] Meagher (1975).
[11] Frentrup (1980).
[12] Cahay et al. (1981).
[13] This work, *R*—least-squares refinement.

Pyrope crystals often contained both solid and liquid inclusions less than 10 μm in size, the former especially in those synthesized from oxides. The solid inclusions generally could not be identified because of their small grain size. Olivine and quartz were detected in several pyrope crystals during microprobe analysis. The inclusions were concentrated in the cores, whereas the rims were mostly clear and almost free of inclusions. Inclusion patterns of the type shown in Figure 1 are sometimes, but not always present. These inclusions and the zonation of the OH^- contents in some samples (see below) made estimation of the refractive indices difficult. Therefore the refractive indices were not used as a measure of the OH^- contents (Ackermann et al., 1983).

The X-ray measurements and refinements, together with data available in the literature (Table 2), show that there is a slight increase in the cell dimension (a_o) of pyrope grown hydrothermally compared to polycrystalline pyrope synthesized anhydrously from a glass (Geiger et al., 1988). The stoichiometries of representative pyrope crystals determined from electron microprobe analyses are listed in Table 3. Crystals synthesized at lower pressure (i.e., <30 kbar) generally display garnet stoichiometries, within the errors of the analyses, but those synthesized at higher pressure (>40 kbar) were generally slightly alumina deficient and magnesia enriched relative to pure pyrope. Alumina-deficient synthetic pyropes were also noted by Charlu et al. (1975). If a majorite component ($Mg_4Si_4O_{12}$) were responsible for this effect, the silica would also be elevated to the same extent as the magnesia con-

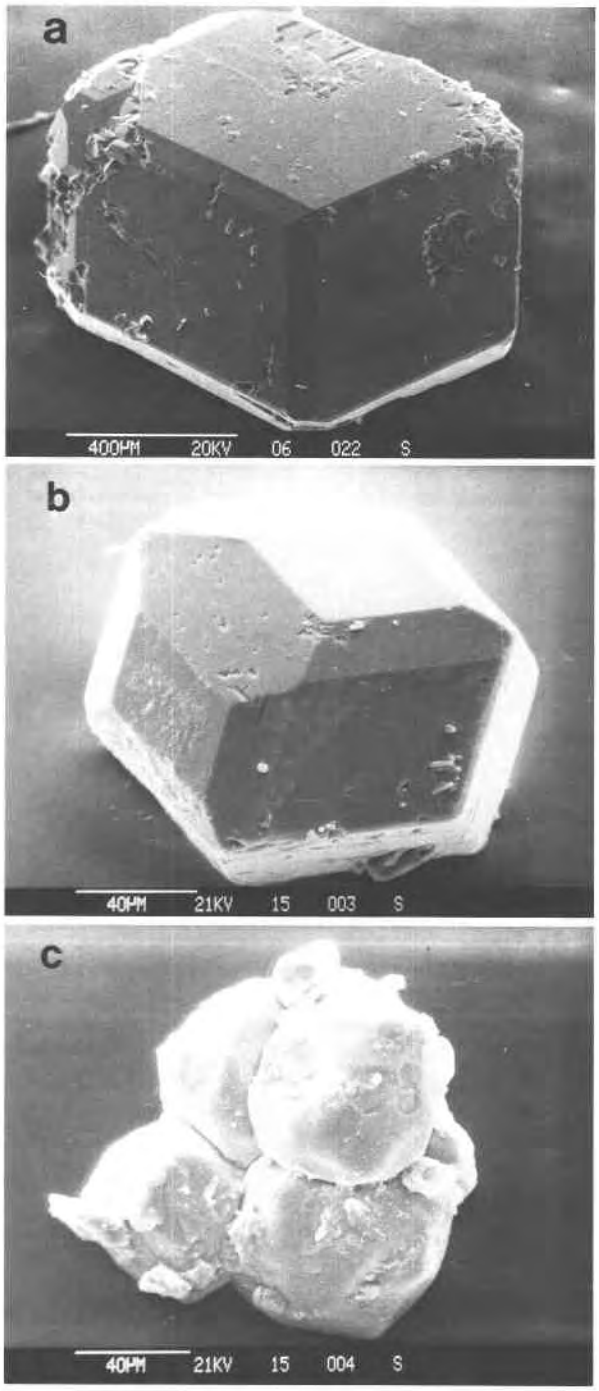

Fig. 2. SEM photographs of representative pyrope single crystals grown from (a) an oxide mixture (P-5), (b) a glass (P-7), and (c) a gel (P-8). All three syntheses were made at 1000 °C and 22.9 kbar, using equal proportions of solids and H_2O. The scales are shown in the lower left.

←

tents. Systematic variation (i.e., zonation) in the stoichiometries was not observed in core to rim traverses.

The IR spectra taken on optically clear parts of the crystals showed no variation in the number of bands or their position in all of the pyropes grown from oxides. In the room-temperature measurements only a single asymmetric OH^- stretching vibration was observed. The position of this band was 3629 $cm^{-1} \pm 2$ cm^{-1} regardless of the pressure and temperature of synthesis and composition of the fluid flux (i.e., 1 N NaOH, HCl, or H_2O) employed. Figure 3 shows a FTIR spectrum obtained on a large pyrope single crystal grown at 900 °C and 30 kbar. Also shown for comparison is the IR spectrum of a pyrope crystal grown in dilute HCl (Fig. 4). The spectra shown in Figures 3 and 4 were taken using measuring spots of 20 and 100 μm respectively. The bottom spectrum in Figure 4 is corrected for the H_2O held in very small fluid inclusions. To do this, a spectrum was first obtained from a thin film of H_2O squeezed between two glass slides. The H_2O spectrum was then subtracted from the pyrope spectrum. The OH^- band shapes in both spectra are slightly asymmetric with full widths at half-height (FWHH) of 60 $cm^{-1} \pm 5$ cm^{-1}. Both spectra agree with the St-1 spectrum presented by Ackermann et al. (1983), except for the band position, 3600 cm^{-1}, which was less certain in the latter case. In many spectra a broad absorption band centered at approximately 3425 cm^{-1} was observed (Fig. 4). The intensity of this band was greater in those regions where more fluid inclusions could be observed (Ackermann et al., 1983). This band varied greatly in intensity and sometimes dwarfed the OH^- stretching vibration. In Figure 3 it is not present.

Measurements made at 78 K showed the presence of two narrow (FWHH = 11 cm^{-1}) absorption bands with peak positions at 3638 cm^{-1} and 3614 cm^{-1}. Figure 5 is a comparison of the room-temperature and 78 K spectra of the same pyrope crystal. The slight corrugation present in the spectra is related to interference effects. The intensity ratio of the two bands is about 3.3 to 1.

In contrast to the single crystals grown from oxides, those pyrope crystals synthesized from the gel, at temperatures lower than 1000 °C, display a four band spectrum with narrow bands at 3665, 3651, 3641, and 3618

Table 3. Electron microprobe analyses of representative pyrope single crystals

Sample/ crystal no.	Average stoichiometry	Standard deviation Mg	Al	Si	Number of points
P-54/1	$Mg_{3.08}Al_{1.93}Si_{3.01}O_{12}$	0.03	0.01	0.02	15
P-13/1	$Mg_{3.00}Al_{2.00}Si_{3.00}O_{12}$	0.01	0.01	0.01	10
P-29/1	$Mg_{2.98}Al_{1.97}Si_{3.04}O_{12}$	0.02	0.01	0.01	6
P-18/1	$Mg_{2.99}Al_{1.99}Si_{3.02}O_{12}$	0.03	0.01	0.01	25
P-57/1	$Mg_{3.06}Al_{1.93}Si_{3.01}O_{12}$	0.05	0.02	0.02	11
P-44/1	$Mg_{3.01}Al_{1.97}Si_{3.02}O_{12}$	0.02	0.01	0.01	8
P-77/1	$Mg_{3.01}Al_{1.94}Si_{3.04}O_{12}$	0.03	0.02	0.08	5
DB-31	$Mg_{3.02}Al_{2.00}Si_{2.99}O_{12}$	—	—	—	3

Note: All analyses normalized to 12 O atoms.

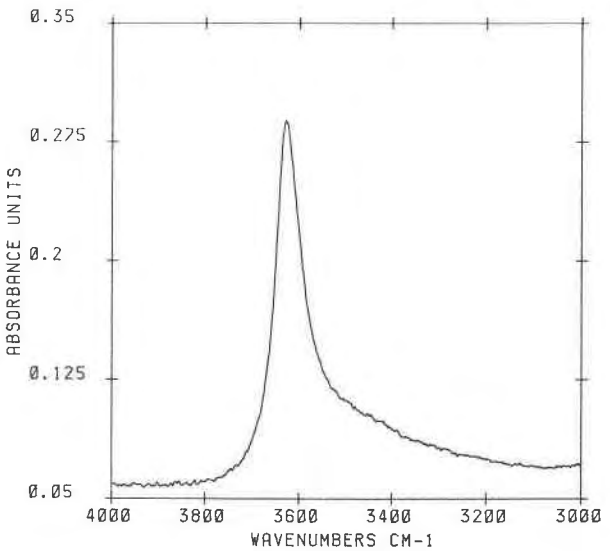

Fig. 3. FTIR microscope spectrum of a pyrope (P-90a) at 298 K with a single band at 3629 cm^{-1}. The crystal is 324 μm thick and the measurement was made at a resolution of 4 cm^{-1} with a measuring diameter of 20 μm.

and a shoulder at 3604 cm^{-1}, with respective FWHH of 12, 6, 11, 10, and 10 cm^{-1} estimated by eye (Fig. 6). This spectrum was not observed in any pyrope crystals grown from oxides or glass. Crystals grown from gel at 1000 °C gave variable results. Crystals grown at Berlin gave the four band spectrum, whereas crystals grown at Pasadena gave the single band pattern. One major difference between the two syntheses was the time the experiments were held at T and P (Table 1).

Variations in the absorbance values of the 3629 cm^{-1}

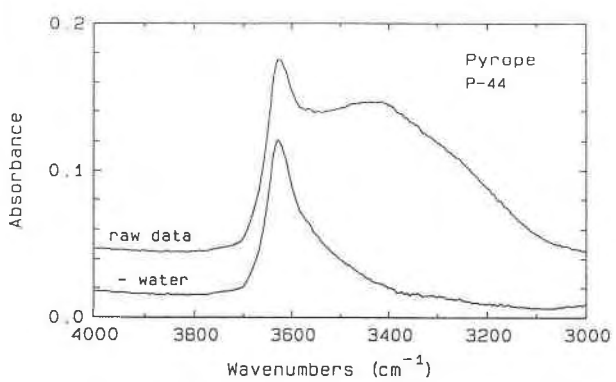

Fig. 4. IR spectra of a pyrope single crystal (P-44) grown in dilute HCl. The top spectrum is the actual measured spectrum which shows a broad H_2O band around 3425 cm^{-1}, and the OH^- stretching band due to structurally incorporated OH^- groups at 3629 cm^{-1}. The bottom spectrum shows the single OH^- stretching band after the broad H_2O band has been subtracted. The crystal is 341 μm thick and the measurements were made on the Nicolet spectrometer using an aperture of 100 μm at a resolution of 4 cm^{-1}.

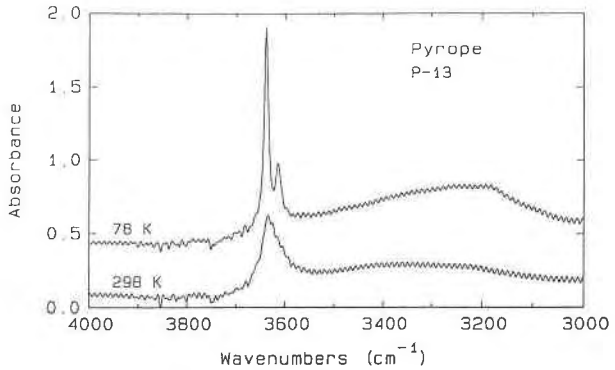

Fig. 5. Comparison of the IR spectrum of pyrope (P-13) at 78 K (above) and at room temperature (below). The crystal is 272 μm thick; the measurements were made using an aperture of 160 μm at a resolution of 4 cm^{-1}. The high frequency oscillations are due to interference fringes.

band indicate that the OH^- content in the crystals changes as a function of pressure and temperature of synthesis. However, we have not been able to establish a simple systematic variation of the OH^- content as a function of pressure and temperature of synthesis. Complications are related to two factors. First, the OH^- content depends upon the starting material used in the synthesis. The OH^- content is higher in pyrope grown from a glass or gel compared to pyrope grown from oxides. In the garnets grown from gel the amount of OH^- is roughly four to five times higher than those grown from oxides at T, P conditions around 1000 °C and 23 kbar. Huckenholz and Fehr (1982) have observed that in synthetic hydrogrossular garnets the hydrogarnet component decreases at a given temperature, with different starting materials, decreasing from glass to oxide to hydroxide mix to condensed gel to (anhydrous) grossular. They also noted that the initially formed composition could not be reequilibrated at high temperatures in short experimental durations. Second, IR profiles measured across our samples show that the OH^- content is sometimes, but not always, greatest in the core and decreases toward the rim (Fig. 7). The above discrepancies among the different starting materials and lack of systematic correlations between P and T and OH^- content indicate that there are problems in obtaining equilibrium products.

To test the proposal of Begley and Sclar (1985) that OH^- containing pyropes are unstable at 1-atm and lose OH^- with time, we measured the IR spectrum of P-51 on the same rim location 1 yr after the first measurements. We observed absolutely no change in the intensity of the single OH^- stretching vibration.

Discussion

Crystal growth

The synthesis work and optical and SEM studies suggest that pyrope growth is a complex process. Crystal size is governed by the nature of the starting material, with

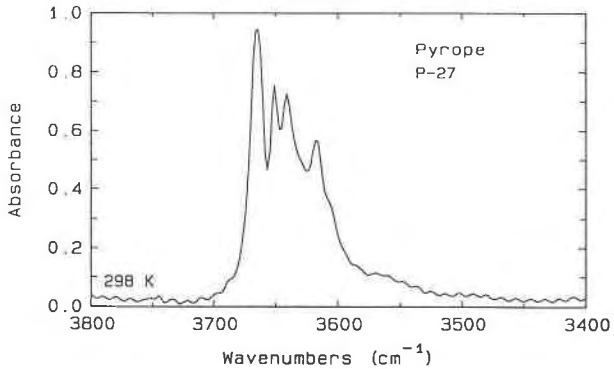

Fig. 6. IR spectrum of pyrope P-27 synthesized from a gel and normalized to 1 mm thickness. The measurement was made on the Nicolet spectrometer. The four bands are located at 3665, 3651, 3641, and 3618 cm^{-1}, with a shoulder at 3604 cm^{-1}.

the larger crystals being produced from oxides, which should be the least reactive starting material compared to either the glass or gel. When glass or gel starting materials are employed, a large number of pyrope crystals nucleate sooner and grow faster than pyrope crystals grown from oxides. The crystals produced are also more homogeneous as demonstrated by the higher abundance of solid phase inclusions in the single crystals grown from oxides. Temperature, pressure, and experimental duration are also factors in crystal growth rates and product sizes, but no simple relationship could be found in the experiments made here. Nucleation effects are also surely important, but poorly understood at the present time. Crystal growth probably occurs relatively rapidly immediately after nucleation and then proceeds more slowly toward the rims. This is consistent with both the higher concentration of inclusions and OH^- found in the cores (Figs. 1 and 7), compared to the clear rims. The crystals

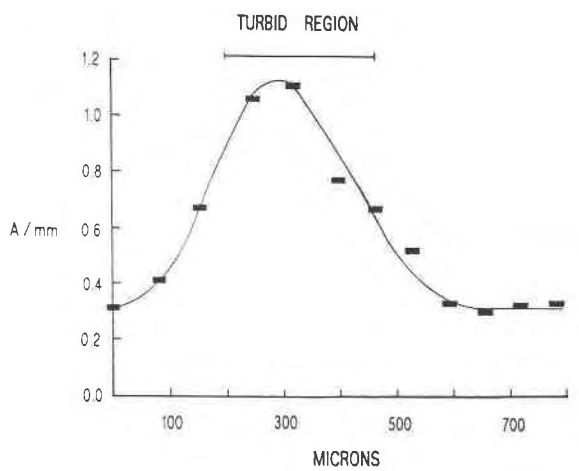

Fig. 7. A plot of the absorbances per millimeter of the OH^- stretching band measured across a single crystal of 800 μm width (DB-31) from rim to rim.

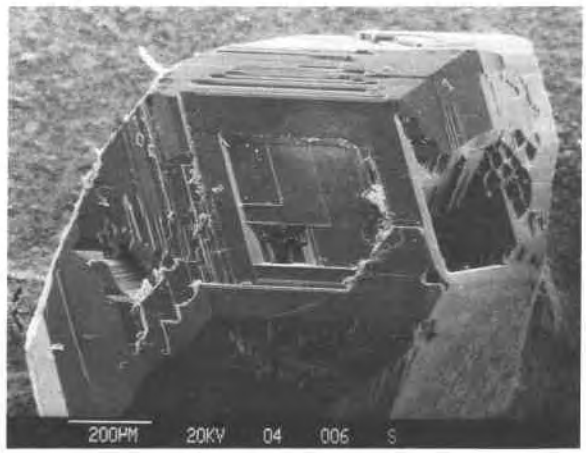

Fig. 8. SEM photograph showing growth steps on a euhedral pyrope single crystal (P-90) synthesized hydrothermally at 900 °C and 30 kbar for 48 h. The top crystal face grew alongside the wall of the capsule. The scale is at the bottom left.

grown from glass also contain more tiny fluid inclusions compared to the oxide-grown crystals.

It appears that pyrope growth from oxides occurs slowly in concentric step layering as opposed to a sector growth process. The SEM photo of the single crystal shown in Figure 8 displays growth zoning steps which are suggestive of an isotropically outwardly growing crystal.

FTIR spectroscopy and location of the OH^- groups

The IR spectroscopic data obtained for pyrope crystals grown from oxides, which show the single sharp IR band at 3629 cm^{-1}, are best interpreted as indicating that the OH^- is indeed incorporated in the classic hydrogarnet substitution, where a cluster of $(O_4H_4)^{4-}$ replaces a SiO_4^{4-} tetrahedral group of point symmetry $\bar{4}$. The room temperature IR measurements made on completely clear and inclusion-free parts of the crystals display the same spectra regardless of the P and T of synthesis and the composition of the fluid phase (H_2O, NaOH, or HCl). There is no change in the position of the single OH^- band. The possibility that submicroscopic inclusions could be responsible for this band at 3629 cm^{-1} was given careful thought. However, we were unable to match the IR spectra of pyrope single crystals grown from oxides with those of known hydrous phases in the system MgO-Al_2O_3-SiO_2-H_2O. Furthermore, the intensity of the OH^- band does not increase in regions of the crystals with dense concentrations of observable inclusions. These observations suggest that the OH^- is structurally bound in pyrope and the IR spectra are not related to submicroscopic inclusions or alteration products. Figure 9 shows the IR spectrum taken on polycrystalline pyrope synthesized dry from a glass (Haselton and Westrum, 1980). No absorption bands are present in the OH^- stretching region; the spectrum is featureless except for the presence of interference effects. Therefore the OH^- band is not a surface related effect made during grinding and polishing of the crystals. This

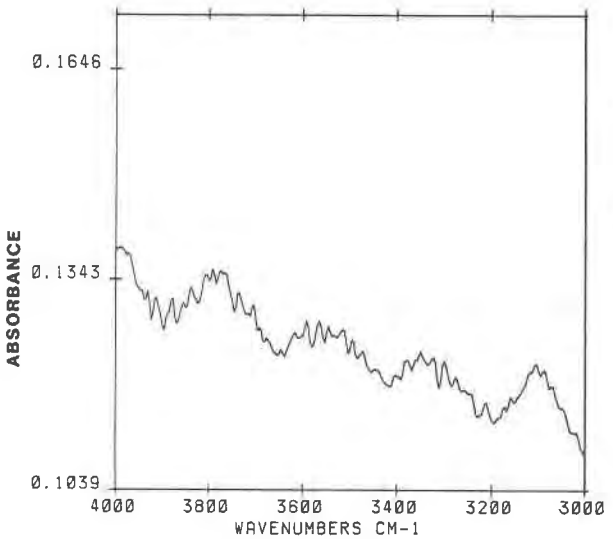

Fig. 9. IR spectrum taken on polycrystalline pyrope synthesized dry from a glass. No OH^- bands are present. Measurements were made on a polycrystalline chip of 75 μm thickness, prepared for spectroscopy in the same way as the synthetic OH-bearing pyrope crystals, at a resolution of 8 cm^{-1} using a microscope spectrometer with 1500 total scans.

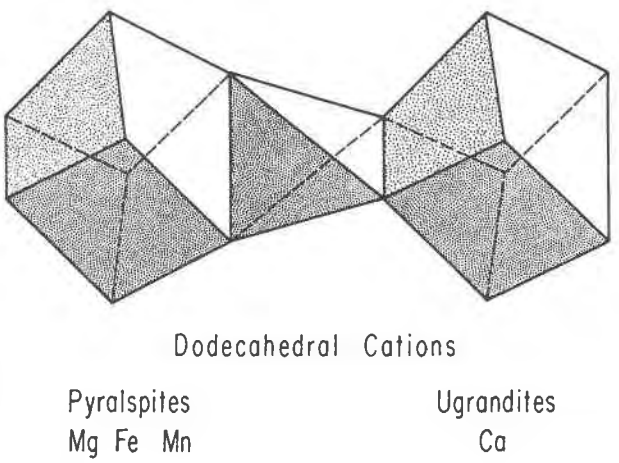

Fig. 10. Polyhedral diagram of part of the garnet structure showing two dodecahedral sites that share edges with a single tetrahedral site, which in the case of the hydrogarnet substitution consists of $(O_4H_4)^{4-}$ (reproduced from Aines and Rossman, 1984b).

further proves that the 3629 cm^{-1} band is not some other feature of the spectrum of pyrope such as an overtone of a Si-O motion.

The low-temperature IR measurements show two distinct OH^- stretching bands (Geiger et al., 1989b). The room temperature spectra display an asymmetry that suggests the possible presence of two overlapping bands which might separate at the lower temperatures. Harmon et al. (1982) calculated the number of IR active bands that are present in tetrahedral, T_d, clusters of the type H_4X_4, where X = Cl, F, or O. They predict that under D_{2d} or S_4 symmetry a T_2 band should split into B_2 + E (D_{2d}) or B + E (S_4) and one should observe two bands in the OH^- stretching region. S_4 is the symmetry of the tetrahedral site in the aluminosilicate garnets (Menzer, 1926; Meagher, 1980) and in hydrogrossular (Cohen-Addad et al., 1967) as determined from X-ray and neutron diffraction studies. The suggestion that a single absorption band is characteristic of the hydrogarnet substitution in pyrope (Ackermann et al., 1983) is only true at room temperature conditions. The apparent single band spectrum at room temperatures demonstrates the need for making low-temperature measurements in these types of studies. Typical spectra of natural pyrope garnets observed by Aines and Rossman (1984b) show two bands in the OH^- region at approximately 3660 and 3560 cm^{-1}. The difference in frequency and relative intensities of the bands between natural and synthetic samples suggests that the mode of OH^- substitution differs in these two types of samples, although this interpretation is complicated by the chemical complexity of natural pyrope samples.

The narrow widths (FWHH) of the two bands observed at 78 K reflect, in part, the absence of different nearest or next-nearest neighbor interactions that are present in the natural garnets. The effect of adding additional components in natural garnets is not only to shift the positions of the OH^- bands, but also to increase their widths (see Aines and Rossman, 1984b). This has been demonstrated in IR studies of the lattice vibrations of natural and synthetic garnets (Moore et al., 1971; Geiger et al., 1989c), which show vibrational coupling between the tetrahedral and dodecahedral sites in garnet (see Fig. 10).

The IR spectrum of synthetic hydrogrossular $[Ca_3Al_2(O_4H_4)_3]$ displays a single asymmetric OH^- band at room temperature that splits at 4 K into two major components at 3680 and 3590 cm^{-1} (Cohen-Addad et al., 1967). At 10 K only one band is observable (Harmon et al., 1982). In the latter study the hydrogarnet substitution was verified by neutron diffraction and H^+-NMR methods.

Room temperature FTIR spectra from single crystals of hydrothermally prepared synthetic almandine ($Fe_3Al_2Si_3O_{12}$) also display two OH^- stretching bands. At 78 K their positions are 3617 and 3595 cm^{-1}, with FWHH of 11 and 9 cm^{-1} respectively. The spectrum is similar in appearance to the 78 K pyrope spectrum (Geiger et al., 1989a). The energy difference between the two bands is the same within experimental error, namely 24 cm^{-1} for pyrope and 22 cm^{-1} for almandine but is much smaller than the value of 90 cm^{-1} observed for hydrogrossular. However, the relative intensities of the two bands appear to be different: 4.8 to 1 in almandine and 3.3 to 1 in pyrope. It is difficult to make definitive statements regarding the locations of the H^+ atoms, but Cohen-Addad et al. (1967) measured an O-H length of 0.93 to 0.95 Å from low-temperature neutron diffraction data. The structures of pyrope and almandine are the most similar

of the aluminosilicate garnets, and therefore it should be expected that their IR spectra should be similar. However, it is not clear why the room temperature spectrum of almandine displays two IR active OH^- stretching bands. One explanation may lie in the low atomic displacement factors which have been observed in single crystal X-ray studies of synthetic almandine relative to pyrope and grossular (Armbruster et al., unpublished data). Thermal and/or positional atomic disorder in pyrope and grossular may act to blur the double band spectra at room temperature.

It is difficult to interpret the four band spectrum observed in certain pyrope crystals crystallized from gel. No band is present at 3629 cm^{-1} and nothing similar was observed in pyrope crystals grown from the oxides. It is possible that submicroscopic hydrous inclusions could be responsible for the additional bands or that the mode of OH^- incorporation is different in these pyrope crystals. It is possible that OH^- incorporation is faster in pyrope grown from gel and additional substitutions such as $^{[6]}Al^{3+} + 3O^{2-} = {}^{[6]}\square + 3OH^-$, $^{[8]}Mg^{2+} + 4OH^- = {}^{[8]}\square + 2OH^-$, $^{[6]}Al^{3+} + O^{2-} = {}^{[6]}Mg^{2+} + OH^-$ or $^{[4]}Si^{4+} + O^{2-} = {}^{[4]}Al^{3+} + OH^-$ may play a role in introducing very small amounts of OH^- in the pyrope structure.

Estimates of OH^- concentrations

The absolute concentrations of OH^- in pyrope can, in principle, be measured using Beer's Law

$$A = \epsilon \cdot t \cdot c \qquad (1)$$

where A is defined as the absorbance and can be measured directly from the spectrum, ϵ is the molar absorptivity of OH^- and is dependent upon the material measured, t is thickness in cm, and c is the concentration in mole l^{-1}. The problem in using Equation 1 for H_2O determination arises from the necessity to know ϵ. It is necessary to obtain independent estimates of the absolute H_2O contents using other techniques (e.g., Rossman et al., 1988) that can then be used to calibrate the IR spectrum. We can estimate the OH^- contents in the synthetic pyropes using the value of ϵ, which is known for OH^- bearing natural grossulars (Rossman and Aines, in preparation). Assuming that ϵ is the same for pyrope and grossular, we calculate that the pyrope in Figure 3 contains 0.05 wt% H_2O. In general, the H_2O contents range from 0.02 to 0.07 wt% for pyrope crystals grown from oxides.

The OH^- contents can also vary considerably within a single crystal. Figure 7 shows an IR traverse from rim to rim, through the core, of a 800 μm pyrope crystal, DB-31, grown in the continual presence of H_2O. The absorbance varies by a factor of almost four from the rim compared to a turbid region located toward the center of the crystal. This bell-shaped profile is consistent with the idea that rapid pyrope nucleation and growth occurred initially and incorporated nonequilibrium amounts of structural OH^-, followed by slower crystal growth and incorporation of less OH^- probably approaching equilibrium concentrations near the edges or rim of the crystal. The OH^- contents appear to level off toward the edges of the crystal. This profile also indicates that the kinetics of the exchange $(O_4H_4)^{4-} = SiO_4^{4-}$ in garnet crystals is very slow even at elevated temperatures (i.e., >1000 °C).

A single OH^- stretching vibration was also observed in pyrope single crystals which were grown in the presence of excess silica (P-51 and P-77). The hydrogarnet component at the rims of single crystals grown from oxides is likely to be a stable equilibrium component fixed at P and T and governed by the relation

$$Mg_3Al_2(SiO_4)_3 + 2x\ H_2O = Mg_3Al_2(SiO_4)_{3-x}[(OH)_4]_x + xSiO_2 \qquad (2)$$

Hydrothermally grown pyrope crystals cannot be stoichiometric, $Mg_3Al_2(SiO_4)_3$, however anhydrous pyrope can be synthesized from anhydrous glass precursors. Work is in progress wherein we are attempting to determine the OH^- contents on a number of crystals grown over a wide range of P and T and f_{H_2O} through careful IR profiling analyses, but ultimately equilibrium will need to be demonstrated by reversal experiments. Moreover, Equilibrium 2 is dependent upon the activity of SiO_2 and this should be buffered during pyrope growth.

The amount of OH^- that can be held in pyrope is much less than in grossular, which forms a complete solid solution with hydrogrossular (Flint et al., 1941; Huckenholz and Fehr, 1982). The low OH^- contents in pyrope may be dictated by the "intrinsic instability" of the structure as discussed by Lager et al. (1989). The amount of inflation of a_o for OH^- containing pyrope is very small ranging from about 0.002 to 0.004 Å (Table 2). Begley and Sclar (1985) reported a much larger increase in a_o (≈0.2 Å), which was not reproduced in these measurements. The smallest a_o value of 11.454 Å was obtained on pyrope synthesized dry from a glass and contains no structural OH^- (see Fig. 9—however see data of Newton et al., 1977 and Wood, 1988). The cell dimension data for pyrope are, therefore, also consistent with a small hydrogarnet substitution. Care must be placed in quantitative interpretation of the unit-cell data because of possible zonation in the crystals and the possible presence of a majorite component in the higher pressure syntheses.

The low absolute amounts of OH^- may be controlled crystallochemically by the edge-sharing structural arrangement between the tetrahedral sites and dodecahedral sites as shown in Figure 10. In strictly anhydrous pyrope the dodecahedral site is too large for the small Mg cation, as evidenced by the large displacement factor (i.e., B = 0.789) which has been observed for Mg in X-ray diffraction experiments (Novak and Gibbs, 1971). Addition of a hydrogarnet component into pyrope forces the dodecahedral site to expand and this is not structurally or energetically favorable in comparison with grossular as argued by Zabinski (1966). Lager et al. (1989) have used distance-least-squares modeling to simulate the effect of the $(O_4H_4)^{4-} = (SiO_4)^{4-}$ substitution on the garnet structure. These calculations indicate that the substitu-

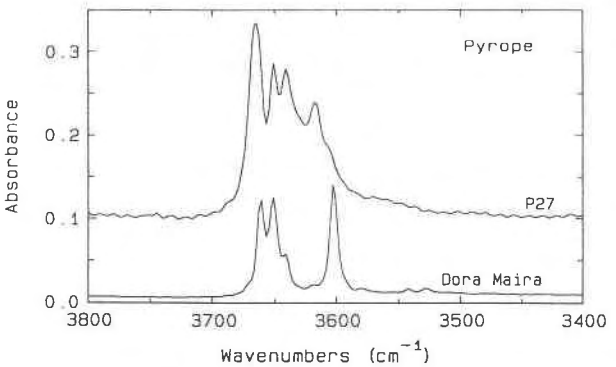

Fig. 11. IR spectra of pyrope P-27 (above) grown from gel compared to the spectrum of the Dora Maira pyrope (below—Rossman et al., 1989). Both spectra are normalized to 1 mm thickness (see text for band energies).

tion may be controlled by the relative lengths of shared and unshared octahedral-dodecahedral bond lengths and that in pyrope a large degree of the hydrogarnet substitution will lead to a structurally and energetically unfavorable situation. Based on a simple size consideration of the dodecahedral cation, it can be expected that the amount of hydrogarnet component will decrease in the series grossular, spessartine, almandine, and finally pyrope (i.e., decreasing size of the divalent cation) at a given pressure, temperature, and f_{H_2O}.

Applications to natural pyrope garnets

A desirable goal for further study would be to measure quantitatively the OH^- contents of natural pyrope crystals and to make inferences regarding the values of f_{H_2O} during garnet growth. If the substitution of OH^- in natural pyrope is as in hydrogarnet, then the prospect for such measurements is favorable because it is likely that the measured OH^- contents are those recording mantle equilibration conditions and not reequilibration conditions attained during rapid ascent to the Earth's surface. This view is justified by the stable OH^- profiles observed in our synthetic crystals. OH^- is not unstable and easily lost from the pyrope structure as proposed by Begley and Sclar (1985).

Rossman et al. (1989) have recently measured the IR spectrum of a nearly end-member pyrope found in the high pressure coesite-bearing metapelites of the Dora Maira Massif of the Alps. The characteristic IR spectrum of this pyrope is radically different from either the spectra of natural pyrope-rich garnets of mantle origin or synthetic pyrope grown from oxides, but it is similar to the spectra shown in Figure 6. It is a four band pattern with sharp narrow bands located at 3662, 3651, 3641, and 3602 cm^{-1}, with FWHH of 3.9, 5.7, 5.3, and 3.7 cm^{-1} respectively (Fig. 11). The highest energy bands in both differ by only 4 cm^{-1}, which is slightly greater than the uncertainty, while the three lower energy bands have analogous counterparts in the pyrope crystals grown from gel. It is probable that the OH^- held in the Dora Maira pyrope and the synthetic pyrope with four bands is located in several different structural sites. The absolute OH^- contents, however, are at least an order of magnitude lower in the Dora Maira pyrope (0.0032 to 0.00016 wt%) than the ones studied by Aines and Rossman (1984a) and also in our synthetics.

Bell and Rossman (in preparation) have also measured the IR spectra on a large number of mantle-derived pyrope crystals taken from South African kimberlites which show more complicated spectroscopic features than those published earlier (Aines and Rossman, 1984a). The same is also true for natural grossular garnets, where many different IR spectra have been observed (Rossman and Aines, in preparation). It is clear that OH^- incorporation into natural garnets is a more complicated structural process than in the chemically simple end-member garnets.

Acknowledgments

We would like to thank H. Reuff for skillful preparation of the sample mounts. D. Ackermand at Christian Albrechts University, Kiel and F. Galbert at Zelmi of the Technische Universität Berlin helped in the microprobing. H. Newesely generously assisted in making the SEM photos at the Free University in Berlin. Some of the high pressure syntheses were done at the Ruhr University through the courtesy of W. Schreyer and H.J. Massonne. We also thank P.J. Wyllie for access to the high pressure facility at Caltech. C.R. Ross II made some of the initial X-ray refinements. We gratefully acknowledge financial support by the Deutsche Forschungsgemeinschaft, Bonn–Bad Godesberg under grant La 324/25, and the National Science Foundation (USA) grant EAR-8618200. Gerlind Siebeker carefully typed the final version of the manuscript.

References cited

Ackermann, L., Cemič, L., and Langer, K. (1983) Hydrogarnet substitution in pyrope: A possible location for "water" in the mantle. Earth and Planetary Science Letters, 62, 208–214.

Aines, R.D., and Rossman, G.R. (1984a) Water content of mantle garnets. Geology, 12, 720–723.

——— (1984b) The hydrous component in garnets: Pyralspite. American Mineralogist, 69, 1116–1126.

Akaogi, M., and Akimoto, S. (1977) Pyroxene-garnet solid solution equilibria in the systems $Mg_4Si_4O_{12}$-$Mg_3Al_2Si_3O_{12}$ and $Fe_2Si_4O_{12}$-$Fe_3Al_2Si_3O_{12}$ at high pressures and temperatures. Physics of the Earth and Planetary Interiours, 15, 90–106.

Basso, R., Cimmino, F., and Messiga, B. (1984) Crystal chemistry of hydrogarnets from three different microstructural sites of a basaltic metarodingite from the Voltri Massif (Western Ligura, Italy). Neues Jahrbuch für Mineralogie Abhandlung, 3, 246–258.

Begley, A.L., and Sclar, C.B. (1984) Experimental evidence for the existence of hydropyrope. Eos, 65, 1091.

——— (1985) High-pressure hydrothermal synthesis of hydrogen-bearing pyrope garnet. 2nd International Symposium on hydrothermal reactions, Program and Abstracts, 36.

Cahay, R., Tarte, P., and Fransolet, A.-M. (1981) Interprétation du spectre infrarouge de variétés isotopiques de pyropes synthétiques. Bulletin de Minéralogie, 104, 193–200.

Cemič, L., Geiger, C.A., Hoyer, H., Koch-Müller, M., and Langer, K. (1990) Piston-cylinder techniques: Pressure and temperature calibration of a pyrophyllite-based assembly by means of DTA measurements, a salt-based assembly, and a cold sealing sample encapsulation method. Neues Jahrbuch für Mineralogie Monatshefte, 2, 49–64.

Charlu, T.V., Newton, R.C., and Kleppa, O.J. (1975) Enthalpies of formation at 970 K of compounds in the system MgO-Al_2O_3-SiO_2 from high temperature solution calorimetry. Geochimica et Cosmochimica Acta, 39, 1487–1497.

Cohen-Addad, C., Ducros, P., and Bertaut, E.F. (1967) Etude de la substitution du groupement SiO_4 par $(OH)_4$ dans les composes $Al_2Ca_3(OH)_{12}$ et $Al_2Ca_3(SiO_4)_{2.16}(OH)_{3.36}$ de type grenat. Acta Crystallographica, 23, 220–230.

Flint, E.P., McMurdie, H.F., and Wells, L.S. (1941) Hydrothermal and X-ray studies of the garnet-hydrogarnet series and the relationship of the series to hydration products of portland cement. Journal Research National Bureau of Standards, 82, 213–219.

Frentrup, K.-R. (1980) Absorptionsspektren von synthetischen Silikatgranaten und Granatmischkristallen und ihre Anwendung zur spektroskopischen 3d-Ionenanalyse in Granaten, 216 p. Ph.D. dissertation, University of Bonn.

Geiger, C.A., Newton, R.C., and Kleppa, O.J. (1987) Enthalpy of mixing of synthetic almandine-grossular and almandine-pyrope garnets from high-temperature solution calorimetry. Geochimica et Cosmochimica Acta, 51, 1755–1763.

Geiger, C.A., Langer, K., Winkler, B., and Cemič, L. (1988) The synthesis, characterization and physical properties of end-member garnets in the system $(Fe,Mg,Ca,Mn)_3Al_2(SiO_4)_3$. In H. Vollstädt, Ed., High pressure geosciences and material synthesis, p. 193–198, Akademie-Verlag, Berlin.

Geiger, C.A., Lager, G.A., Amthauer, G., Richardson, J.F., and Armbruster, T. (1989a) Almandine garnet: Synthesis, structure, and Mössbauer and NIR spectroscopy (abs). 12th European Crystallographic Meeting, Moscow USSR, 2, 6.

Geiger, C.A., Langer, K., Bell, D.R., and Rossman, G.R. (1989b) Realbau of pyrope single crystals grown hydrothermally (abs.). International Conference Crystal structure, microstructure and properties of minerals and ceramic materials, Bochum University, FRG, 55–56.

Geiger, C.A., Winkler, B., and Langer, K. (1989c) Infrared spectra of synthetic almandine-grossular and almandine-pyrope garnet solid-solutions: Evidence for equivalent site behaviour. Mineralogical Magazine, 53, 231–237.

Harmon, K.M., Gabriele, J.M., Nuttall, A.S. (1982) Hydrogen bonding in the tetrahedral $O_4H_4^{4-}$ cluster in hydrogrossular. Journal of Molecular Structure, 82, 213–219.

Haselton, H.T., and Westrum, E.F. (1980) Low temperature heat capacities of pyrope, grossular, and $pyrope_{60}$ $grossular_{40}$. Geochimica et Cosmochimica Acta, 44, 701–709.

Hazen, R.M., and Finger, L.W. (1978) Crystal structures and compressibilities of pyrope and grossular to 60 kbar. American Mineralogist, 63, 277–303.

Huckenholz, H.G., and Fehr, K.T. (1982) Stability relationships of grossular + quartz + wollastonite + anorthite II. The effect of grandite-hydrograndite solid solution. Neues Jahrbuch für Mineralogie Abhandlung, 145, 1–33.

Lager, G.A., Armbruster, T., Rotella, F.J., and Rossman, G.R. (1989) The OH substitution in garnets: X-ray and neutron diffraction, infrared and geometric modelling studies. American Mineralogist, 74, 840–851.

Massonne, H.-J., and Schreyer, W. (1986) High-pressure syntheses and X-ray properties of white micas in the system K_2O-MgO-Al_2O_3-SiO_2-H_2O. Neues Jahrbuch für Mineralogie Abhandlung, 153, 177–215.

Meagher, E.P. (1975) The crystal structures of pyrope and grossularite at elevated temperatures. American Mineralogist, 60, 218–228.

——— (1980) Silicate garnets. Mineralogical Society of America Reviews in Mineralogy, 11, 25–66.

Menzer, G. (1926) Die Kristallstrukture von Granat. Zeitschrift für Kristallographie, 63, 157–158.

Moore, R.K., White, W.B., and Long, T.V. (1971) Vibrational spectra of the common silicates: I. The garnets. American Mineralogist, 56, 54–71.

Newton, R.C., Charlu, T.V., and Kleppa, O.J. (1977) Thermochemistry of high pressure garnets and clinopyroxenes in the system CaO-MgO-Al_2O_3-SiO_2. Geochimica et Cosmochimica Acta, 41, 369–377.

Novak, G.A., and Gibbs, G.V. (1971) The crystal chemistry of the silicate garnets. American Mineralogist, 56, 791–825.

Rossman, G.R. (1988) Vibrational spectroscopy of hydrous components. Mineralogical Society of America Reviews in Mineralogy, 18, 193–204.

Rossman, G.R., Rauch, F., Livi, R., Tombrello, T.A., Shi, C.R., and Zhou, Z.Y. (1988) Nuclear reaction analysis of hydrogen in almandine, pyrope, and spessartine garnets. Neues Jahrbuch für Mineralogie Monatshefte, 4, 172–178.

Rossman, G.R., Beran, A., and Langer, K. (1989) The hydrous component of pyrope from the Dora Maira Massif, Western Alps. European Journal of Mineralogy, 1, 151–154.

Schreyer, W., and Seifert, F. (1969) High-pressure phases in the system MgO-Al_2O_3-SiO_2-H_2O. American Journal of Science, 267-A, 407–443.

Sekine, T., Wyllie, P.J., and Baker, D.R. (1981) Phase relationships at 30 kbar for quartz eclogite composition in CaO-MgO-Al_2O_3-SiO_2-H_2O with implications for subduction zone magmas. American Mineralogist, 66, 938–950.

Skinner, B.J. (1956) Physical properties of end-members of the garnet group. American Mineralogist, 41, 428–436.

Wood, B.J. (1988) Activity measurements and excess entropy-volume relationships for pyrope-grossular garnets. Journal of Geology, 96, 721–729.

Zabinski, W. (1966) Hydrogarnets. Polska Akademia Nauk, Oddzial Krakowie, Komisja Nauk Mineralogicznych, Prace Mineralogiczne, 3, 1–69.

Manuscript received October 9, 1989
Manuscript accepted November 7, 1990